Desalination and Water Treatment
www.deswater.com

doi:10.5004/dwt.2019.23948

153 (2019) 65–75
June

Rapid removal of boron from environmental water samples using magnetic graphene oxide: optimized by central composite design

Nour Al-Afy[a,b], Hassan Sereshti[a,*]

[a]*School of Chemistry, University College of Science, University of Tehran, Tehran, Iran, Tel. +98-21-66495291, Fax +98-21-6113735, email: sereshti@ut.ac.ir, sereshti@khayam.ut.ac.ir (H. Sereshti)*
[b]*Doctoral School of Science and Technology, Research Platform for Environmental Science (PRASE), Lebanese University, Lebanon, email: nour.alafy@ut.ac.ir, nour.aliii2010@gmail.com (N. Al-Afy)*

Received 20 September 2018; Accepted 11 February 2019

ABSTRACT

In the present study, magnetic graphene oxide nanocomposite (GO/Fe_3O_4) was synthesized and used as an efficient adsorbent for the removal of boron from water samples. The removal efficiency was checked using inductively coupled plasma optical emission spectrometry (ICP-OES). The adsorbent was characterized by field emission scanning electron microscopy (FESEM), X-ray diffraction (XRD), Fourier transform infrared (FTIR) spectroscopy, and vibrating sample magnetometry (VSM). The effective parameters of adsorption process including pH, adsorbent dosage, and contact time were optimized using a central composite design (CCD). Under the optimal conditions (pH 9.2, adsorbent dose of 82 mg, and contact time of 14.8 min), the relative standard deviation was 1.87% (C=100 mg L^{-1}, n=9) with the determination coefficient (R^2) of 0.9980. The maximum adsorption capacity of GO/Fe_3O_4 was 35.7 mg g^{-1}. The adsorption isotherm was well fitted with the Langmuir model. Finally, the method was applied to remove boron in tap, mineral and groundwater samples and satisfactory removal efficiencies (95–97%) were obtained.

Keywords: Boron; Magnetic graphene oxide; Inductively coupled plasma optical emission spectroscopy; Central composite design; Adsorption isotherm models

1. Introduction

Boron is a nonmetallic element that is widely distributed in the environment [1]. It is an important micro nutrient for humans, plants, and animals. Moreover, it occurs as a significant component in various industries such as glass, steel, ceramics, porcelain, cosmetics, carpets, semiconductors and fireproofing fabrics [2]. Boron mainly exists in the form of boric acid (H_3BO_3) or borate anions ($B(OH)_4^-$) in nature [3]. The average concentration of boron is approximately 10 mg kg^{-1} in the earth crust [4], 30 mg kg^{-1} in the soil, 4.5 mg kg^{-1} in seawater, and 0.3–100 mg kg^{-1} in groundwater [5]. With the frequent use of this volatile element, the increase in the boron waste could lead to the pollution of drinking water sources. When discharged to the environment, it may volatilize and return to the ground in the form of acid rainfall, and enters into the soil, and then could be adsorbed by plants [1]. Eventually, the drinking water sources will be polluted which could lead to a series of health and environmental problems. Parks et al. asserted that the acceptable daily intake of boron is 18 mg/d for an average body weight of 60 kg [3]. The World Health Organization [6] has set 2.4 mg L^{-1} as a guideline value for boron concentration in drinking water while 1.0 mg L^{-1} is the recommended content for drinking water by the European Union [3].

For such reasons, many methods, such as co-precipitation [7], coagulation [8], solvent extraction [9], membrane operations [10] and adsorption [11] have been developed for boron removal from water and wastewater. Among these methods, the adsorption technique is the most popular and widely used simple which is simple, cost-effective,

*Corresponding author.

a compatible procedure for removal of boron from aqueous solutions. Different materials such as fly ash [12], activated carbon [13], resins [10], composite magnetic particles [14], and multi-walled carbon nanotube [15] have been used as adsorbent for the removal of boron from aqueous solutions. Graphene, a type of one or several atomic layered graphites, possesses special two-dimensional structure (2D) composed of a single layer of sp^2 networks of carbon atoms arranged in a honeycomb pattern with excellent thermal, mechanical, and electrical properties [16]. Graphene oxide (GO), which is considered as the oxidized graphene, contains oxygen-containing functional groups such as –COOH, –C=O, and –OH on its surface. These groups are essential for high sorption of heavy metal ions [17].

Lately, magnetic nanoparticles, mainly Fe_3O_4, have appeared as efficient advanced composite materials due to their simplicity and ease in recovering adsorbent from the liquid phase using an external magnetic field [18]. However, pure magnetic nanoparticles may suffer from some inherent limitations as agglomeration that results in their magnetic properties in complex matrices [19]. Thus, these nanometer-sized metal oxides are not suitable for samples with complicated matrices [20]. To overcome such limitations, modification of Fe_3O_4 to produce an efficient nanocomposite is required. In the current work, magnetic GO/Fe_3O_4 nanocomposite was synthesized by co-precipitation of iron salts onto graphene oxide nanosheets and used for the removal of boron before ICP-OES analysis. The removal procedure was optimized with response surface methodology.

2. Materials and methods

2.1. Reagents and materials

The graphite powder was purchased from Samchun Pure Chemical Co., Ltd. (Pyeongtaek, Korea). Potassium permanganate ($KMnO_4$), ferrous chloride tetrahydrate ($FeCl_2{\cdot}4H_2O$), ferric chloride hexahydrate ($FeCl_3{\cdot}6H_2O$), concentrated sulfuric acid (H_2SO_4, 98%), hydrogen peroxide (H_2O_2), hydrochloric acid (HCl), nitric acid (HNO_3), and sodium nitrate ($NaNO_3$), ammonia NH_3 (25%), boric acid H_3BO_3, sodium fluoride (NaF), and all other reagents were purchased from Merck Chemicals (Darmstadt, Germany). The stock solution of boron (1000 mg L^{-1}) was prepared by dissolving 0.573 g of H_3BO_3 in 1 L of buffered solution of pH 9.2 and stored at 4°C until use. Dilute solutions were prepared by appropriate dilution of stock solutions in double distilled water (DDW). For determination of boron in aqueous samples, only plastic lab-ware should be used from the time of sample collection to the completion of the analysis. The laboratory plastic ware was washed with double distilled water before applications.

2.2. Apparatus

A Varian Vista-MPX ICP-OES (Canberra, Australia) equipped with a slurry nebulizer and a charge coupled device (CCD) detector was used for determination of samples. The instrument parameters and the related emission line of boron are given in Table S1 (supplementary data file). X-ray diffraction (XRD) analysis of the synthesized GO/Fe_3O_4 was carried out by a Philips Analytical Diffractometer X' Pert Pro system, MPD model (Amsterdam, Netherlands) with Cu Kα irradiation (λ = 1.54 Å) operated at 40 kV and 40 mA. The infrared spectrum of GO/Fe_3O_4 was obtained with a Fourier transformed infrared spectrometer (FTIR) from Bruker instruments, Equinox 55 model (Bremen, Germany) in the wavenumber range of 400–4000 cm^{-1} using KBr discs. The morphology of GO/Fe_3O_4 nanosheets was investigated by an FE-SEM using a Hitachi S-4160 machine (Tokyo, Japan) equipped with energy dispersive X-ray spectroscopy (EDX) operated at 5.0 kV. The pH values were measured with a WTW Inolab 720 pH meter (Weilheim, Germany). The magnetic property of the adsorbent was studied using a vibrating sample magnetometer (VSM/AGFM Meghnatis Daghigh Kavir Co., Kashan, Iran) at room temperature. A Eurosonic 4D (Euronda, Montecchio Precalcino (Vincenza) Italy) ultrasonic water bath was employed for dispersion of GO. An orbital shaker (GFL-Gesellschaft für Labortechnik mbH, Burgwedel, Germany) was used to accelerate the adsorption process. Designing the experiments for CCD, analyzing and modeling the data, analysis of variance and constructing the related plots were performed by using a trial version of the "Design-Expert 7.1.3" software package (Stat-Ease Inc., Minneapolis, USA).

2.3. Synthesis of adsorbent

Graphene oxide (GO) was prepared from natural graphite powder by a modified Hummers method [17]. Briefly, 2 g natural graphite powder and 2 g $NaNO_3$ were added to 100 mL H_2SO_4 (98%, w/w) under vigorous stirring at room temperature for 2 h. Then, 12 g $KMnO_4$ was added slowly into the solution in an ice bath. Next, the mixture was heated and refluxed for 12 h, and then cooled to room temperature. In the next step, 20 mL of H_2O_2 (30%) was gradually dropped in the resulting bright yellow colored solution. After that, the mixture was washed several times with HCl/water to remove any inorganic salts until, and finally, dried in an oven at 60°C.

Chemical co-precipitation of Fe(II) and Fe(III) in alkaline solution was used for the preparation of magnetite GO [21]. Firstly, 0.5 g of GO was dispersed in 40 mL of deionized water under sonication for 30 min. Under a nitrogen atmosphere, 0.94 g of $FeCl_2{\cdot}4H_2O$, 2.5 g of $FeCl_2{\cdot}6H_2O$ and 50 mL of deionized water were added to the mixture with vigorous stirring. The temperature of the mixture was increased to about 85°C, with an immediate addition of 7.5 mL of NH_3 (25%) under vigorous stirring for 45 min. Then, the mixture was cooled with continuous stirring until room temperature. After that, the obtained black sediment was washed three times using deionized water and dried in an oven at 60°C.

2.4. The procedure

At first, 80 mg of GO/Fe_3O_4 was added into 30 mL of a buffered sample solution (pH 9.2) containing 100 mg L^{-1} of boron. Then, the mixture was shaken for 15 min on an orbital shaker at 200 rpm. Next, the adsorbent was separated using an external magnet and the supernatant was analyzed by ICP-OES for determination of boron residue.

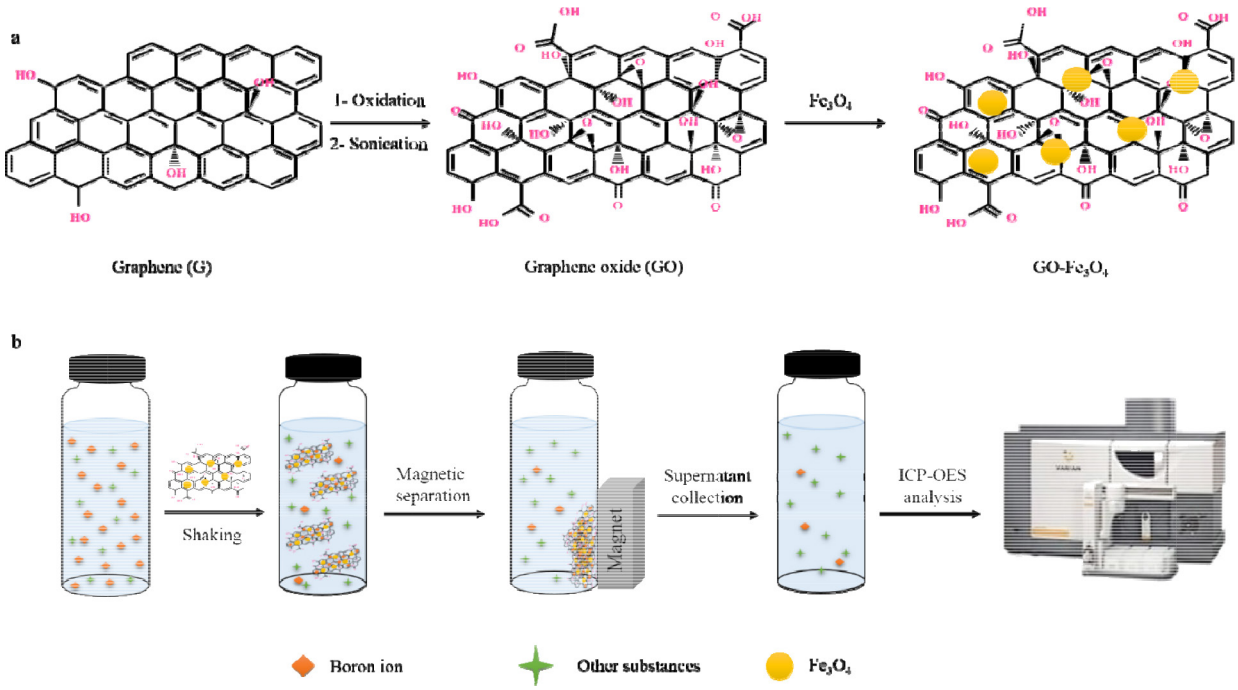

Fig. 1. Scheme of (a) adsorbent synthesis steps; (b) the removal procedure.

The adsorption capacity, amount of the adsorbed boron per unit of adsorbent mass was calculated using the following equation:

$$q_e = \frac{\left(\left(C_i - C_f\right)V\right)}{m} \quad (1)$$

where q_e is the adsorption capacity (mg g^{-1}), C_i is the initial boron concentration (mg L^{-1}), C_f is the residual boron concentration (mg L^{-1}), m is the adsorbent dose (g) and V is the sample volume (L).

3. Results and discussion

3.1. Characterization

The FESEM micro-graphs of GO and GO/Fe_3O_4 are shown in Fig. 2a. Fig. 2a shows a clear difference between the surface morphology of GO and the adsorbent GO/Fe_3O_4. The GO surface has a layered and sheet like structure with a large thickness, wrinkled edge, and smooth surface. While GO/Fe_3O_4 possess a rough surface due to the presence of Fe_3O_4 nanoparticles that have been appeared as bright spots distributed on the surface of GO sheets. According to the micro-graph, the mean diameter of Fe_3O_4 nanoparticles is approximately 50 nm using the Digimizer software package version 4.1.1.0, MedCalc Software (bvba, Mariakerke, Belgium). The elemental analysis data of GO/Fe_3O_4 is shown in Fig. 2b in which the peaks related to the elements such as carbon (C), oxygen (O), and iron (Fe) can be observed.

The FTIR spectra of GO and GO/Fe_3O_4 are displayed in Fig. 2c. As can be seen, the spectrum of GO shows a broad-band at 3450 cm^{-1} related to O–H stretching vibrations. The C=O and C=C stretching vibrations can be observed at 1738 and 1620 cm^{-1}, respectively. The C–O stretching vibrations of epoxy and alkoxy groups have appeared at 1223 and 1051 cm^{-1}, respectively. In the FTIR spectrum of GO/Fe_3O_4 a new absorption band around 578 cm^{-1} that can be ascribed to Fe–O stretching vibrations, confirms the existence of Fe_3O_4 on the surface of GO nanosheets [22].

The XRD analysis was used to investigate the phase and structure of the synthesized GO/Fe_3O_4. As shown in Fig. 2d, the XRD plot of GO reveals a sharp peak at 2θ = 10.12 corresponding to the (002) reflection of GO. This indicates that the inter-planar spacing was increased due to the oxidation treatment, while the weak wide peak at 2θ = 21° suggests residual unoxidized graphite. Moreover, the XRD pattern of GO/Fe_3O_4 shows the peaks at 2θ = 30.1°, 35.9°, 43°, 54°, 57.2° and 63.1° related to the (220), (311), (400), (422), (511), and (440) reflections, respectively. This is in a close concordance with characteristic reflections of the pure cubic spinel crystal structure of Fe_3O_4 (JCPDS No. 19-629).

The magnetic property of GO-Fe_3O_4 was measured by VSM technique at room temperature. As can be seen in Fig. 2e, a high saturation magnetization amount of 55.8 emu g^{-1} was observed for the adsorbent. Where the magnetic hysteresis curve is S-like and passes through the zero point of magnetization with no coercivity nor remanence, suggesting a super paramagnetic property of adsorbent.

3.2. Central composite design optimization

A rotatable and orthogonal central composite design (CCD) was employed to obtain the conditions at which the best possible response is achieved. The rotatability provides constant variance of the predicted response with the same distance from the center of the design, wherein

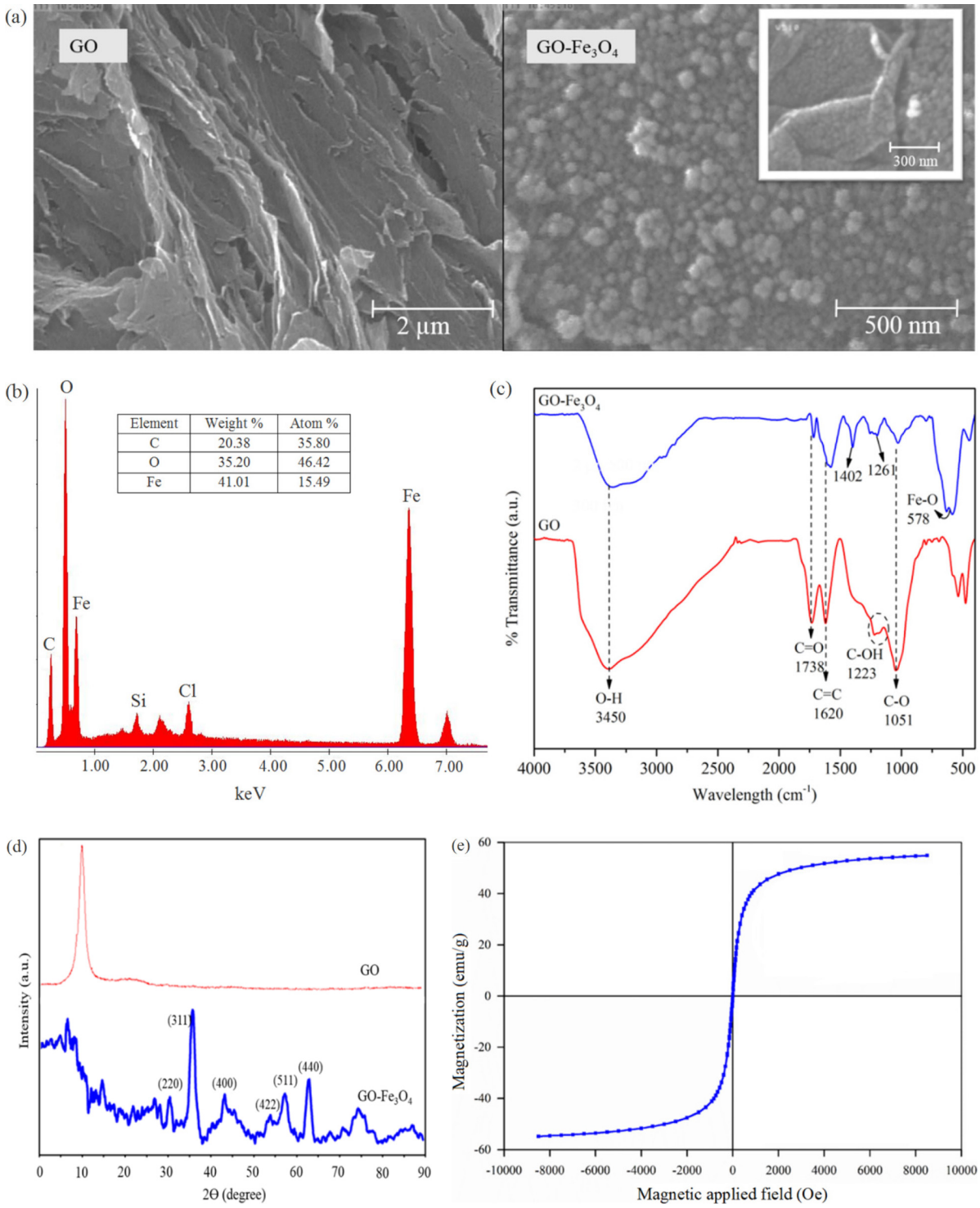

Fig. 2. Characterization of the graphene oxide (GO) and magnetic graphene oxide (GO/Fe_3O_4): (a) SEM images; (b) EDX analysis of GO-Fe_3O_4; (c) FTIR spectrum; and (d) XRD pattern of GO and GO-Fe_3O_4.; (e) VSM magnetization curve of GO-Fe_3O_4.

orthogonality each factor is evaluated independently from all other factors. The design is a combination of a factorial design ($N_f = 2^f$) (f is the number of the factors), a set of center points (N_0), and axial points ($N\alpha = 2f$). Center points are usually repeated to get a good estimate of experimental error (pure error) [23]. The pH (P), adsorbent dose (M), and contact time (t) were recognized as the main parameters of the boron ion removal. Therefore, f is equal to 3. The axial points are located at +α and -α from the center of the experimental domain. The value of the axial point "α" needed to ensure the rotatability is equal to ±1.682 obtained from Eq. (2).

$$\alpha = \sqrt[4]{N_f} \quad (2)$$

Then, N_0 was obtained using Eq. (3) equal to ~9.

$$\alpha = \sqrt{\frac{\sqrt{\left(N_f + N_\alpha + N_0\right)N_f} - N_f}{2}} \quad (3)$$

The total number of experiments (N) needed to run the CCD was calculated using Eq. (4) equal to 23.

$$N = N_f + N_\alpha + N_0 \quad (4)$$

In order to minimize the effect of uncontrolled factors, the experiments were randomized. The experiments were divided into two blocks and carried out in two sequential days to remove the expected variations caused by some changes during the course of the experiments [23]. The main factors, their symbols, and levels are given in Table 1. The experimental design matrix consisted of the number and order of the experiments, levels of the factors in each experiment and the related responses are shown in Table S2 (supplementary data file).

Analysis of variance (ANOVA) (95% confidence level) was considered to evaluate the model and the significance of the effects (Table 2). The F-values show that the model is significant and the lack of fit is not significant relative to the pure error, hence confirm the validity of the model. Where Significant effects should have "probe > F" values less than 0.0500. In this case, P, t, M, Pt, PM, tM, P^2, t^2, and M^2 were the significant effects. The second order polynomial with the most reasonable statistics was considered as the satisfactory response surface model to fit the experimental data. This model [Eq. (5)] consisted of three main effects (P, t, and M), three two-factor interaction effects (Pt, PM, and tM), and three curvature effects (P^2, t^2, and M^2) as follows:

$$\begin{aligned} Y &= b_0 + b_1P + b_2t + b_3M + b_4Pt + b_5PM + b_6tM + b_7P^2 \\ &\quad + b_8t^2 + b_9M^2 \\ &b0=10.45;\ b1=-1.96;\ b2=0.3;\ b3=-2.10;\ b4=1.06;\ b5=0.75;\ b6 \\ &\quad =-0.47;\ b7=-0.8;\ b8=-0.29;\ b9=-0.69. \end{aligned} \quad (5)$$

where Y is the response (boron removal percentage), b_0 is the intercept and the other b terms ($b_1 - b_9$) are the coefficients. The sign of each coefficient (+ or –) shows the direction of the relationship between the related effect and the response. Where if the sign is positive, the effect and the response changes in the same direction, while for the negative sign the response operates in the opposite direction to the effect. The absolute amount of the coefficients measures the strength of the relationship.

Table 1
Factors, their symbols and levels for the central composite design

Factor	Symbol	Level				
		$-\alpha^a$	-1^b	0^c	$+1^d$	$+\alpha^e$
pH	P	2	4.25	6.5	8.75	11
Time (min)	t	2	16.5	31	45.5	60
Adsorbent (mg)	M	10	32.5	55	77.5	100

[a]Minimum axial point. [b]Minimum level. [c]Central value. [d]Maximum level. [e]Maximum axial point.

Table 2
Analysis of variance (ANOVA) for the central composite design

Source	Sum of squares[a]	df[b]	Mean square[c]	F- value[d]	p-value	
					Prob > F[e]	
Block	0.83	1	0.83			
Model	145.89	9	16.21	656.24	< 0.0001	Significant
P[f]	52.11	1	52.11	2109.76	< 0.0001	
T[g]	1.22	1	1.22	49.29	< 0.0001	
M[h]	59.97	1	59.97	2427.75	< 0.0001	
Pt	9.01	1	9.01	364.57	< 0.0001	
PM	4.49	1	4.49	181.97	< 0.0001	
tM	1.79	1	1.79	72.35	< 0.0001	
P^2	1	9.54	386.11	386.11	< 0.0001	
t^2	1	1.29	52.10	52.10	< 0.0001	
M^2	1	7.24	293.02	293.02	< 0.0001	
Residual[i]	0.3	12	0.03			
Lack of fit[j]	0.02	5	4.26×10^{-3}	0.11	0.9868	Not significant
Pure error[k]	0.28	7	0.04			
Cor total[l]	147.01	22				

[a]Sum of the squared differences between the average values and the overall mean. [b]Degrees of freedom. [c]Sum of squares divided by d_f. [d]Test for comparing model variance with residual (error) variance. [e]Probability of seeing the observed F-value if the null hypothesis is true. [f]pH. [g]Time. [h]Mass of adsorbent. [i]Consists of terms used to estimate experimental error. [j]Variation of the data around the fitted model. [k]ariation in the response in replicated design points. [l]Totals of all information corrected for the mean.

The quality of the polynomial model was expressed by the coefficient of determination (R^2, *adjusted*-R^2, and adequate precision). R^2 is a measure of the variations around the mean defined by the model and it is equal to 0.9980. The *adjusted*-R^2 is adapted for the number of terms in the model and it decreases as the number of terms in the model increases whether those additional terms do not add value to the model. Here, it is equal to 0.9965. Adequate precision is a signal-to-noise ratio which compares the range of the predicted values of the design points to the average prediction error. The ratios greater than four elucidate adequate model discrimination. Here it is equal to 85.58.

The effect of factor interactions on the response was also studied using three-dimensional (3D) response surface and counter plots. These plots represent the relationship between the response and the levels of two factors simultaneously, while the third factor is fixed at its central level. Fig. 3a depicts 3D response surface and counter plots of pH-contact time interaction on the boron removal %. As it is obvious, with increasing pH (from acidic to basic conditions) the removal of boron increases. This can be explicated as follows. The pH_{pzc} of GO/Fe_3O_4 is about 3.5 [24] . Therefore, its surface charge is positive at pH < 3.5, and is negative at pH > 3.5 [24]. On the other hand, $B(OH)_3$ with pK_a of 9.2 is the main boron species in the solution at pH < 9.2 and it can bind to hydroxyl ion forming borate anion ($B(OH)_4^-$) [25] (Fig. 4a). In spite of negative surface charge of the adsorbent at pH > 3.5, both boric acid and borate ion react with hydroxyl groups on the surface of GO/Fe_3O_4, resulting in the boric acid ester and the borate monoester, respectively [25] as shown in Fig. 4b. Fig. 3b shows 3D response surface and counter plots of adsorbent dosage-pH on interaction boron % removal. The increase of boron percent removal, with increasing adsorbent amount, can be attributed to the increase of the accessible active sites. Finally, the optimal conditions were obtained based on the model described by Eq. (5) including pH 9.2, contact time 14.8 min, and adsorbent dose of 82 mg.

Repeatability. To study the repeatability of the proposed method, the experiment was repeated for 9 times under

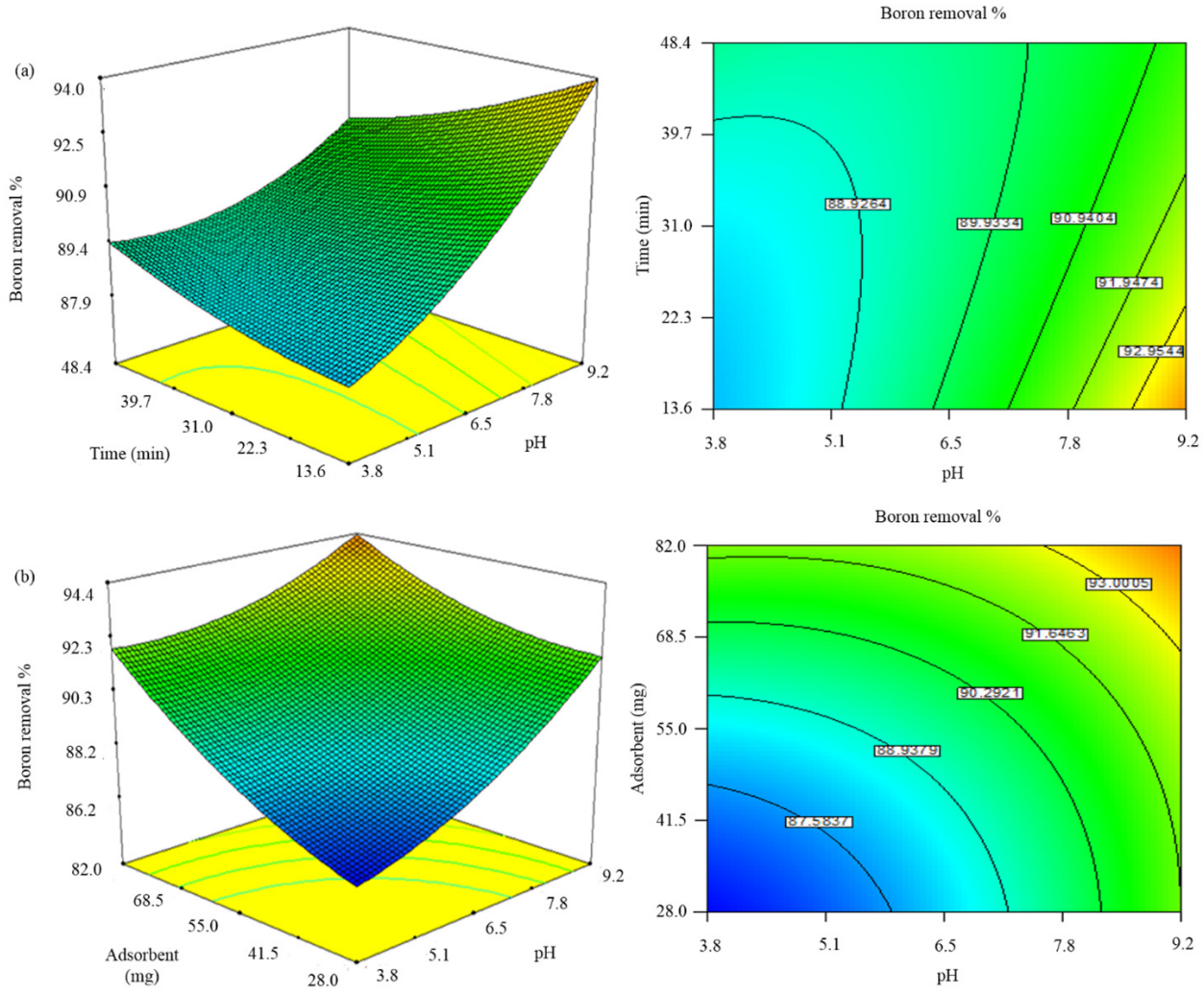

Fig. 3. The 3D response surface and contour plots of (a) the interaction effect of pH-contact time; and (b) pH-Adsorbent dosage on the boron removal percent.

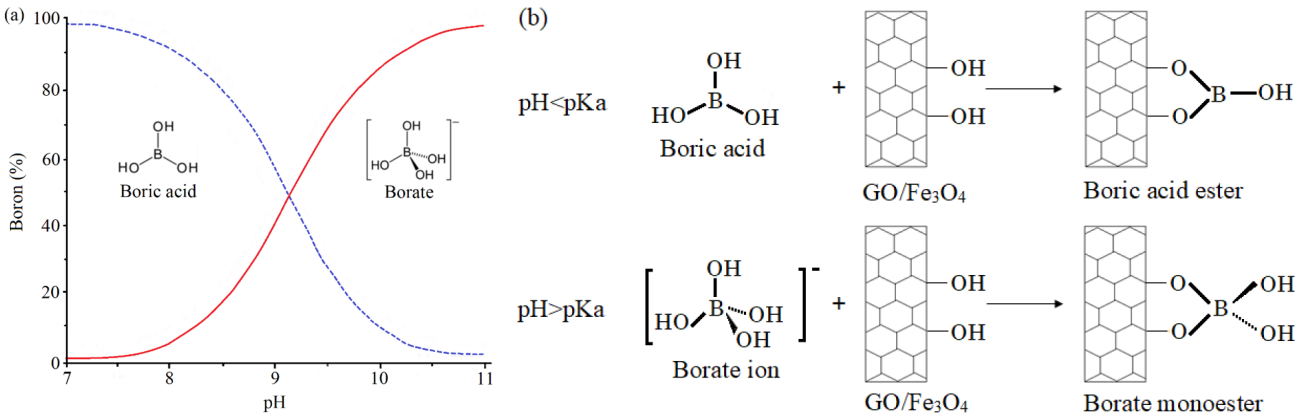

Fig. 4. (a) The behavior and the main boron species in an aqueous solution. (b) Adsorption mechanism of boric acid and borate on GO/Fe_3O_4.

the optimal experimental conditions. The obtained relative standard deviation (RSD, n = 9, C = 100 mg L^{-1}) was 1.87% indicating a good repeatability.

3.3. Effect of coexisting ions

Under the optimum conditions, the effect of various coexisting ions such as K^+, Na^+, Ca^{2+}, Mg^{2+}, Mn^{2+}, Cl^-, CO_3^{2-}, and SO_4^{2-} was investigated with the procedure mentioned in Section 2.4. The data in Table 3 show that the presence of common cations and anions in natural water samples has no significant effect on the removal of boron.

3.4. Re usability of the adsorbent

The reusability is one of the main key parameters that is used to determine the effectiveness of an adsorbent. Accordingly, after the adsorption process was finished, GO/Fe_3O_4 was collected from the solution and washed by NaF solution (0.1 M) for two times, then dried and reused by the proposed procedure. The results showed that the adsorbent can be reused at least 10 times without significant loss of the removal efficiency (<5%). Therefore, GO/Fe_3O_4 has a good capability for repeated use in sample preparation.

3.5. Analysis of real samples

In order to evaluate the applicability of the proposed method for determination of boron, various real water samples including tap, mineral and ground waters were also analyzed with the proposed procedure. The removal percentage (R %) was calculated using the following equation (Eq. (6)):

$$R\% = \left(\frac{(C_f - C_r)}{C_s}\right) \times 100 \quad (6)$$

where C_f, C_r, and C_s are the concentration of boron in the real sample after spiking with boron standard solution, the concentration of boron in unspiked real sample, and the concentration of boron standard solution added to real sample, respectively. The obtained results (Table 4) showed acceptable removal (95–97%) of boron in the real water samples.

Table 3
Effects of interfering ions on the determination of boron

Interfering species	Interference to analyte ratio (w/w)[a]	Boron removal (%)[b]
K^+	2000	97.99
Na^+	2000	97.71
Ca^{2+}	2000	98.6
Mg^{2+}	1000	97.76
Mn^{2+}	500	97.84
Cl^-	2000	96.98
CO_3^{2-}	100	97.85
SO_4^{2-}	100	96.61

[a]Concentration of boron solution is 100 mg L^{-1}. [b]R% = $(C_i - C_f)/C_i \times 100$; R% is the removal %, C_i is the initial concentration of boron (mg L^{-1}) and C_f is the final concentration of boron (mg L^{-1}).

3.6. Adsorption isotherms

In the present study, the Langmuir and Freundlich isotherm models [26] were used to examine the adsorption mechanism of boron onto GO/Fe_3O_4. The Langmuir isotherm assumes monolayer adsorption onto a surface that its linear form is described by Eq. (7):

$$\frac{1}{q_e} = \frac{1}{q_m} + \frac{1}{(q_m K_L C_e)} \quad (7)$$

where q_e is the amount of adsorbed boron per unit mass of the adsorbent at equilibrium (mg g^{-1}), C_e (mg L^{-1}) is the equilibrium concentration of the boron, q_m (mg g^{-1}) is the maximum amount of adsorbed boron per unit mass of the adsorbent to form a complete monolayer on the surface, and K_L is the Langmuir constant related to the affinity of the binding sites (L mg^{-1}). The q_m and K_L were respectively calculated from the intercept and slope of the linear plot of $1/q_e$ versus $1/C_e$ as shown in Fig. 5a. The essential features of the Langmuir isotherm could be assessed in terms of

Table 4
Determination of boron in different real samples

Sample	C_ra (mg L^{-1})	C_f[b] (mg L^{-1})	C_s[c] (mg L^{-1})	RR %[d]
Tap water[d] ± mean SD[e]	n.d.[f]	101.1 ± 0.93	100	97.12
Mineral water ± SD	n.d.	100.24 ± 1.11	100	95.24
Ground water[g]	n.d.	121 ± 0.96	100	96.42
River[h]	n.d.	110.5 ± 0.83	100	96.49

[a]The concentration of boron in unspiked real sample. [b]The concentration of boron in the real sample after spiking with boron standard solution(100 mg L^{-1}). [c]The concentration of boron standard solution added to real sample. [d]The tap water was taken from university of Tehran (Tehran, capital of Iran). [e]Standard deviation (n = 3). [f]Not detected. [g]The water was taken from university of Tehran (Tehran, Iran). [h]The sample was taken from Karaj river (Karag, Iran).

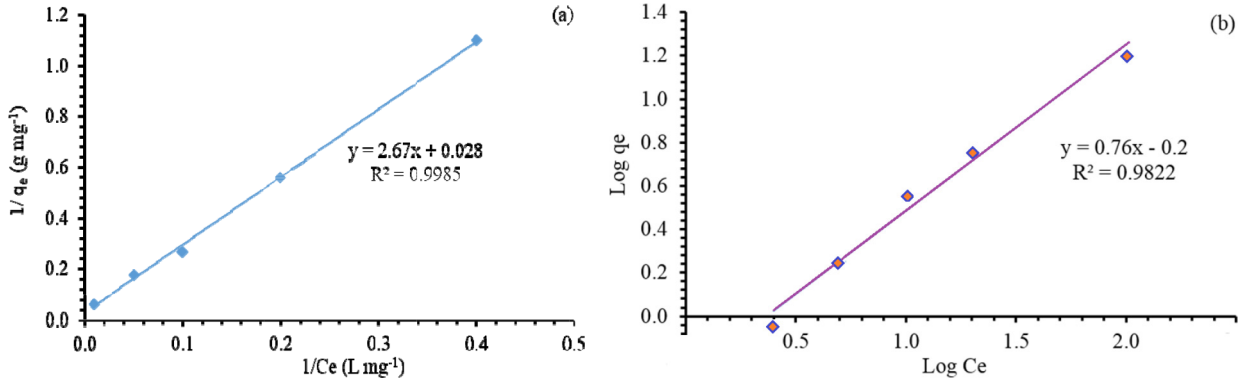

Fig. 5. (a) The Langmuir adsorption isotherm; (b) and the Freundlich adsorption isotherm.

equilibrium parameter R_L (a dimensionless constant called separation factor) [26]:

$$R_L = \frac{1}{\left(1+\left(1+K_L C_0\right)\right)} \tag{8}$$

where C_0 (mg L^{-1}) is the boron initial concentration and R_L indicates the adsorption nature. If $R_L > 1$ the adsorption is unfavorable, if $R_L = 1$ it is linear, if $0 < R_L < 1$ it is favorable, and if $R_L = 0$ the adsorption is irreversible. Herein from the data in, $0 < R_L < 1$, indicating that Langmuir isotherm is favorable (Table 5). However, the Freundlich isotherm can be applied to non-ideal adsorption on heterogeneous surfaces with multilayer adsorption expressed by Eq. (9):

$$\log q_e = \log K_F + \left(\frac{1}{n}\right)\log C_e \tag{9}$$

where C_e indicates the equilibrium concentration of adsorbate (mg L^{-1}), q_e is the amount of adsorbate adsorbed per gram of the adsorbent at equilibrium (mg g^{-1}), K_F is the Freundlich isotherm constant ($mg^{1-(1/n)}\ L^{1/n}\ g^{-1}$), and n represents the adsorption intensity. The K_F and n were determined from the intercept and slope of the plot of log q_e versus log C_e (Fig. 5b). The $1/n$ value ranges between 0 and 1 show the degree of non-linearity between solution concentration and adsorption. A favorable adsorption condition is achieved when $n > 1$. Herein the n value for boron adsorption on GO/Fe_3O_4 was 1.3 (the Freundlich is also adequate for use). Thus, we conclude that both Langmuir and Freundlich equations fit the adsorption results.

The Langmuir and Freundlich models were also evaluated regarding correlation coefficients (R^2) which are used as a measure of goodness of fit to the adsorption models [27]. The R^2 values show that the experimental data well fit with the Langmuir isotherm, which implies a monolayer adsorption of boron on the surface of GO/Fe_3O_4. According to the Langmuir equation, the maximum adsorption capacity for boron was 35.7 mg g^{-1}. The adsorption isotherms were constructed with the procedure in section 2.4 in the concentrations range of 2.5–100 mg L^{-1} boron species.

3.7. Comparison study

A literature survey was made to compare the proposed method with other published methods for boron removal and the results were given in Table 6. The adsorption capacity of GO/Fe_3O_4 and the percent removal was higher than that of the other methods. In addition, the contact time and adsorbent dose are better than most of the other mentioned methods. The results clearly indicate that GO/Fe_3O_4 is more effective and faster than previous studies for the removal of boron from water sample.

4. Conclusions

In the present study, a magnetic graphene oxide nanoparticle (GO/Fe_3O_4) was synthesized and used, for the first time, as an effective adsorbent for the removal of boron from aqueous solutions. The sorption isotherms are fitted better by the Langmuir isotherm suggesting that the

Table 5
Adsorption constants for the Langmuir and Freundlich isotherm models

	Langmuir				Freundlich		
Analyte	K_L [a]	q_m [b]	R_L [c]	R^{2} [d]	n [e]	K_F [f]	R^2
Boron	0.011	35.7	0.32–0.49	0.9985	1.3	0.6	0.9822

[a]Langmuir constant (mg L^{-1}). [b]Maximum adsorption capacity (mg g^{-1}). [c]Separation factor. [d]Correlation coefficient. [e]Adsorption intensity. [f]Adsorption capacity.

Table 6
Comparisons of the adsorption capacities for boron adsorption by different adsorbents

Adsorbent	Analysis	Adsorption capacity (mg g^{-1})	Contact time (min)	R%	Adsorbent (g L^{-1})	Ref.
Fly ash	Flame AAS [g]	6.9	1440	90	750	[12]
AC[a]	UV-vis	0.4	60	40	200	[28]
AC-TA [b]	UV-vis	2.2	60	78.8	200	[28]
AC-M [c]	UV-vis	2	60	73.4	200	[28]
Mg/Al DLH[d]-60	ICP-AES [h], IC [i]	1.2–13.0	240	86.6	36	[29]
Mg/Al DLH-450	ICP-AES, IC	5.4–17.3	240	93.5	16	[29]
Mg–Fe HT[e]	ICP-OES [j]	3.1	10	33	2.5	[30]
Mg–Al HT	ICP-OES	9.2	80	92	2.5	[30]
TA-MWCNT [f]	UV-vis	1.9	60	–	0.3	[15]
GO-Fe_3O_4	ICP-OES	35.7	14.4	95–97	2.7	This work

[a]Activated carbon. [b]Activated C impregnated with tartaric acid. [c]Activated C impregnated with mannitol. [d]Mg/Al double layered hydroxides. [e]Hydrotalcite. [f]Tartaric acid-multi wall carbon nanotube. [g]Atomic absorption spectrophotometer. [h]Inductively coupled plasma atomic emission spectrophotometer. [i]Ion chromatography. [j]Inductively coupled plasma optical emission spectrophotometer.

sorption of boron on GO/Fe_3O_4 nanosheets is of monolayer coverage. To determine the optimum conditions for boron removal using GO/Fe_3O_4, a CCD with the least number of experiments was used. The proposed sorbent presented agreeable stability, re usability, adsorption capacity, and rate of equilibrium for the sorption of boron ions. The method was successfully applied for the determination of boron in the several different water samples with the satisfactory percent removal in the range of 95.24–97.12%.

Acknowledgements

The authors would like to convey grateful thanks to University Tehran, for providing the funding facility to carry out this research work.

References

[1] B. Wang, X. Guo, P. Bai, Removal technology of boron dissolved in aqueous solutions–a review, Colloids. Surf. A. Physicochem. Eng. Asp., 444 (2014) 338–344.
[2] D.E. Garrett, Uses of borates, Borates: Handbook of Deposits, Processing, Properties, and Use. Elsevier 1998, pp. 401–429
[3] J.L. Parks, M. Edwards, Boron in the environment, Crit. Rev. Environ. Sci. Technol., 35 (2005) 81–114.
[4] M. Badruk, N. Kabay, M. Demircioglu, H. Mordogan, U. Ipekoglu, Removal of boron from wastewater of geothermal power plant by selective ion-exchange resins. I. Batch sorption–elution studies, Sep. Sci. Technol., 34 (1999) 2553–2569.
[5] N. Hilal, G.J. Kim, C. Somerfield, Boron removal from saline water: a comprehensive review, Desalination, 273 (2011) 23–35.
[6] WHO (World Health Organization), Guidelines for Drinking-water Quality, 4th ed., Genava, 2014.
[7] M. Turek, P. Dydo, J. Trojanowska, A. Campen, Adsorption/co-precipitation–reverse osmosis system for boron removal, Desalination, 205 (2007) 192–199.
[8] M.H. Isa, E.H. Ezechi, Z. Ahmed, S.F. Magram, S.R.M. Kutty, Boron removal by electro coagulation and recovery, Water Res., 51 (2014) 113–123.
[9] R. Zhang, Y. Xie, J. Song, L. Xing, D. Kong, X.-M. Li, T. He, Extraction of boron from salt lake brine using 2-ethylhexanol, Hydrometallurgy, 160 (2016) 129–136.
[10] A. Alharati, Y. Swesi, K. Fiaty, C. Charcosset, Boron removal in water using a hybrid membrane process of ion exchange resin and micro filtration without continuous resin addition, J. Water Process Eng., 17 (2017) 32–39.
[11] Z. Guan, J. Lv, P. Bai, X. Guo, Boron removal from aqueous solutions by adsorption–A review, Desalination, 383 (2016) 29–37.
[12] I. Polowczyk, J. Ulatowska, T. Koźlecki, A. Bastrzyk, W. Sawiński, Studies on removal of boron from aqueous solution by fly ash agglomerates, Desalination, 310 (2013) 93–101.
[13] S.A. Ganiyu, O.O. Ajumobi, S.A. Lateef, K.O. Sulaiman, I.A. Bakare, M. Qamaruddin, K. Alhooshani, Boron-doped activated carbon as efficient and selective adsorbent for ultra-deep desulfurization of 4, 6-dimethyldibenzothiophene, Chem. Eng. J., 321 (2017) 651–661.
[14] A.A. Oladipo, M. Gazi, Hydroxyl-enhanced magnetic chitosan micro beads for boron adsorption: Parameter optimization and selectivity in saline water, React. Funct. Polym., 109 (2016) 23–32.
[15] N. Zohdi, F. Mahdavi, L.C. Abdullah, T.S.Y. Choong, Removal of boron from aqueous solution using magnetic carbon nanotube improved with tartaric acid, J. Environ. Health Sci. Eng., 12 (2014) 1–12.

[16] S. Mahpishanian, H. Sereshti, Three-dimensional graphene aerogel-supported iron oxide nanoparticles as an efficient adsorbent for magnetic solid phase extraction of organophosphorus pesticide residues in fruit juices followed by gas chromatographic determination, J. Chromatogr., A 1443 (2016) 43–53.
[17] W.S. Hummers Jr, R.E. Offeman, Preparation of graphitic oxide, J. Am. Chem. Soc., 80 (1958) 1339–1339.
[18] R. Hasanzadeh, P.N. Moghadam, N. Bahri-Laleh, M. Sillanpää, Effective removal of toxic metal ions from aqueous solutions: 2-Bifunctional magnetic nanocomposite base on novel reactive PGMA-MAn copolymer@Fe_3O_4 nanoparticles, J. Colloid Interface Sci., 490 (2017) 727–746.
[19] X. Zhao, S. Liu, P. Wang, Z. Tang, H. Niu, Y. Cai, F. Wu, H. Wang, W. Meng, J.P. Giesy, Surfactant-modified flower like layered double hydroxide-coated magnetic nanoparticles for preconcentration of phthalate esters from environmental water samples, J. Chromatogr., A 1414 (2015) 22–30.
[20] E.V. Alonso, M.M.L. Guerrero, P.C. Cueto, J.B. Benítez, J.M.C. Pavón, A.G. de Torres, Development of an on-line solid phase extraction method based on new functionalized magnetic nanoparticles. Use in the determination of mercury in biological and sea-water samples, Talanta, 153 (2016) 228–239.
[21] L. Nyaba, J.M. Matong, P.N. Nomngongo, Nanoparticles consisting of magnetite and Al_2O_3 for ligand less ultrasound-assisted dispersive solid phase micro extraction of Sb, Mo and V prior to their determination by ICP-OES, Microchim. Acta, 183 (2016) 1289–1297.
[22] M.Z. Kassaee, E. Motamedi, M. Majdi, Magnetic Fe_3O_4-graphene oxide/polystyrene: fabrication and characterization of a promising nanocomposite, Chem. Eng. J., 172 (2011) 540–549.
[23] H. Sereshti, V. Khojeh, S. Samadi, Optimization of dispersive liquid–liquid micro extraction coupled with inductively coupled plasma-optical emission spectrometry with the aid of experimental design for simultaneous determination of heavy metals in natural waters, Talanta, 83 (2011) 885–890.
[24] J.H. Deng, X.R. Zhang, G.M. Zeng, J.L. Gong, Q.Y. Niu, J. Liang, Simultaneous removal of Cd(II) and ionic dyes from aqueous solution using magnetic graphene oxide nanocomposite as an adsorbent, Chem. Eng. J., 226 (2013) 189–200.
[25] M. Ruiz, C. Tobalina, H. Demey-Cedeño, J.a. Barron-Zambrano, a.M. Sastre, Sorption of boron on calcium alginate gel beads, React. Funct. Polym., 73 (2013) 653–657.
[26] A.A. Zamani, R. Shokri, M.R. Yaftian, A.H. Parizanganeh, Adsorption of lead, zinc and cadmium ions from contaminated water onto Peganum harmala seeds as biosorbent, Int. J. Environ. Sci. Technol., 10 (2013) 93–102.
[27] N. Al-Afy, A. Hijazi, H. Rammal, M. Reda, R. Nehme, H. Annan, J. Toufaily, T. Hamieh, Removal of cadmium(II) ion from wastewater by using Lebanese Prunus avium stem as adsorbents, Desal. Water Treat., 92 (2017) 215–221.
[28] J. Kluczka, J. Ciba, J. Trojanowska, M. Zolotajkin, M. Turek, P. Dydo, Removal of boron dissolved in water, Environ. Prog., 26 (2007) 71–77.
[29] J.Q. Jiang, Y. Xu, K. Quill, J. Simon, K. Shettle, Laboratory study of boron removal by Mg/Al double-layered hydroxides, Ind. Eng. Chem. Res., 46 (2007) 4577–4583.
[30] O.P. Ferreira, S.G. De Moraes, N. Duran, L. Cornejo, O.L. Alves, Evaluation of boron removal from water by hydrotalcite-like compounds, Chemosphere, 62 (2006) 80–88.

Supplementary

Table S1
Instrumental parameters of ICP-OES and boron ions emission lines

Parameter	Value
RF generator power (kW)	1.3
Plasma gas flow rate (L min^{-1})	15
Auxiliary gas flow rate (L min^{-1})	1.5
Nebulizer pressure (kPa)	150
Torch mode	Axial
Analytical lines(nm)	B (249.772)

Table S2
Design matrix and responses for the central composite design

Run	Block	pH	t (min)	M (mg)	Concentration (mg L^{-1})
1	1	6.5	31	55	10.13
2	1	6.5	31	55	10.21
3	1	6.5	31	55	10.36
4	1	6.5	2	55	9.1
5	1	6.5	31	100	4.98
6	1	6.5	60	55	10.1
7	1	2	31	55	11.49
8	1	6.5	31	55	10.73
9	1	6.5	31	55	10.48
10	1	6.5	31	55	10.45
11	1	6.5	31	10	11.99
12	1	11	31	55	4.91
13	2	3.8	13.6	82	8.99
14	2	9.2	48.4	28	9.98
15	2	3.8	13.6	28	13.84
16	2	9.2	13.6	82	4.55
17	2	3.8	48.4	82	6.61
18	2	9.2	48.4	82	6.24
19	2	6.5	31	55	10.65
20	2	9.2	13.6	28	6.23
21	2	3.8	48.4	28	13.17
22	2	6.5	31	55	10.55
23	2	6.5	31	55	10.34

Table S3
Effects of interfering ions on the determination of boron

Interfering species	Interference to analyte ratio (w/w)[a]	Boron removal (%)[b]
K^+	2000	97.99
Na^+	2000	97.71
Ca^{2+}	2000	98.6
Mg^{2+}	1000	97.76
Mn^{2+}	500	97.84
Cl^-	2000	96.98
CO_3^{2-}	100	97.85
SO_4^{2-}	100	96.61

[a]Concentration of boron solution is 100 mg L^{-1}. [b]$R\% = (C_i - C_f)/C_i \times 100$; R% is the removal %, C_i is the initial concentration of boron (mg L^{-1}) and C_f is the final concentration of boron (mg L^{-1}).